Biomaterials and Biosystems 21 (2026) 100130

Contents lists available at ScienceDirect

Biomaterials and Biosystems

journal homepage: www.elsevier.com/locate/bbiosy

Rapid bone formation and remodeling via vascular infiltration of a hydroxyapatite/collagen nanocomposite beneath the calvarial periosteum

Hanae Arai [a], Masayoshi Uezono [a,*], Masanori Kikuchi [c], Hitoshi Amano [b], Chen Derong [b], Kazuhiro Aoki [b], Keiji Moriyama [a,d]

[a] Department of Maxillofacial Orthognathics, Graduate School of Medical and Dental Sciences, Institute of Science Tokyo, 1-5-45, Yushima, Bunkyo-ku, Tokyo 113-8510, Japan
[b] Department of Basic Oral Health Engineering, Graduate School of Medical and Dental Sciences, Institute of Science Tokyo, 1-5-45, Yushima, Bunkyo-ku, Tokyo 113-8510, Japan
[c] Bioceramics Group, Biomaterials Field, Research Center for Macromolecules and Biomaterials, National Institute for Materials Science, 1-1, Namiki, Tsukuba, Ibaraki 305–0044, Japan
[d] Oral Science Center, Institute of Biomedical Engineering, Institute of Science Tokyo, 1-5-45, Yushima, Bunkyo-ku, Tokyo 113-8510, Japan

ARTICLE INFO

Keywords:
Hydroxyapatite/collagen bone-like nano-composite
Bone remodeling
Bone replacement
Osteoblast osteoclast angiogenesis
VEGF2R
CTHRC1

ABSTRACT

The development of biomaterials that actively promote bone regeneration remains a major challenge in regenerative medicine and dentistry. This study investigated the time-dependent osteogenic potential of an organic-inorganic composite bone filler (hydroxyapatite/collagen bone-like nanocomposite, HAp/Col) using a rat calvarial model, assessed by immunohistochemistry and bone histomorphometry.

By day 3, vascular endothelial growth factor receptor 2 (VEGFR2)-positive cells were detected on the HAp/Col surface, indicating early vascular invasion. By day 5, vascular infiltration had extended into the scaffold, where double staining with tartrate resistant acid phosphatase (TRAP)/ alkaline phosphatase (ALP) revealed osteoclast-mediated material resorption and osteoblast-mediated bone matrix deposition around vascular cavities. By day 7, bone remodeling within HAp/Col was markedly active, with clusters of osteoblasts producing new bone matrix. Outside the scaffold, osteoblasts adhered to its surface and elongated, enhancing bone formation through the space-forming effect of HAp/Col swelling.

Furthermore, collagen triple helix repeat-containing protein 1 (CTHRC1) expression increased progressively from days 3 to 7, as confirmed by immunostaining and qRT-PCR, suggesting its role as a coupling factor between osteoclast activity and osteoblast differentiation.

These findings suggest that HAp/Col is associated with cellular activities related to bone remodeling, including vascular invasion and osteoclast/osteoblast recruitment. HAp/Col demonstrates biocompatibility and in vivo tissue compatibility as a candidate biomaterial for medical and dental applications.

1. Introduction

Hydroxyapatite/collagen bone-like nanocomposite (HAp/Col) is an organic–inorganic composite biomaterial with a nanostructure and an assumed ideal hydroxyapatite-to-collagen weight ratio of 80/20, closely resembling the composition of natural bone[1]. In Japan, a porous HAp/Col scaffold is clinically used as a bone void filler in medical and dental applications due to its excellent bone-forming capacity via the bone remodeling process [2,3]. Beyond repairing bone defects, bone fillers are also expected to promote new bone formation on existing bone surfaces. Such direct augmentation provides several clinical advantages, including increased alveolar ridge volume without invasive grafting procedures and enhanced implant stability [4].

Among its potential clinical applications, HAp/Col is particularly promising in orthodontics. Subperiosteal anchorage devices [5], which provide stable anchorage for tooth movement, typically require 3–4 months to achieve sufficient bone formation at the bone–device interface. To shorten this period, Uezono *et al.* proposed coating these devices with HAp/Col and demonstrated substantial new bone formation with osseointegration within only four weeks in a rat calvarium model, whereas conventional HAp coating showed very limited osteoconduction and bone formation [6]. These findings suggest that

* Corresponding author.
E-mail address: m-uezono.mort@tmd.ac.jp (M. Uezono).

https://doi.org/10.1016/j.bbiosy.2026.100130
Received 18 October 2025; Received in revised form 21 January 2026; Accepted 22 January 2026
Available online 22 January 2026

HAp/Col may facilitate early stabilization of orthodontic devices and broaden their clinical applications.

The biological mechanisms of HAp/Col-induced bone formation have also been explored. Hiratsuka *et al.* investigated the degradation behavior of HAp/Col *in vitro* under different pH conditions and *in vivo* using micro-computed tomography (μCT) and histological analyses in a rat calvarial model[7]. This study revealed time-dependent swelling of HAp/Col in both models and demonstrated that HAp/Col markedly stimulated osteoclast and osteoblast activity, particularly increasing osteoblast numbers in regions slightly distant from the material. However, the precise mechanisms of its replacement by bone tissue and the dynamic interactions between osteoblasts and osteoclasts within HAp/Col remain poorly understood.

In this study, we investigated the time-dependent process of bone replacement by HAp/Col through bone morphometry after implantation beneath the clavicular periosteum.

2. Materials and methods

2.1. Preparation of specimens

HAp/Col samples were prepared according to the method described by Kikuchi *et al.* [1]. Briefly, HAp/Col fibers were synthesized by wet precipitation using a simultaneous titration method and collected by vacuum filtration. The fibers were shaped into disks using a mold by uniaxial pressing and dried by lyophilization. Rectangular beam specimens (1 × 1 × 5 mm) were then prepared from the disks using a medical razor and sterilized with ethylene oxide gas (Fig. 1A).

2.2. Animal experiments

All animal experiments were approved by the Institutional Animal Care and Use Committee of the Institute of Science Tokyo, Japan (approval number: A2024-021A). Eighteen male Sprague–Dawley rats (12 weeks old, 390–460 g) were used. Animals were maintained on a standard diet ad libitum with free access to water. Under general anesthesia induced by a combination of medetomidine (Domitor; Zenoaq, Fukushima, Japan), midazolam (SANDOZ, Bazel, Switzerland), and butorphanol (Betorfar; Meiji, Tokyo, Japan), a midline skin incision was made along the sagittal suture of the calvaria. The subcutaneous tissue was dissected to expose the periosteum. A small incision was made in the periosteum, and a subperiosteal pocket was created using a thin periosteal elevator. The specimen was then placed into the pocket beneath the periosteum on the left parietal bone as previously described (Fig. 1-B). The skin was closed with 5-0 absorbable sutures (Vicryl; Shofu, Kyoto, Japan). Specimens with surrounding tissues were harvested on postoperative days 3, 5, and 7 from six rats per group. Animals were euthanized using carbon dioxide, and samples were collected for subsequent analyses (Fig. 1-C).

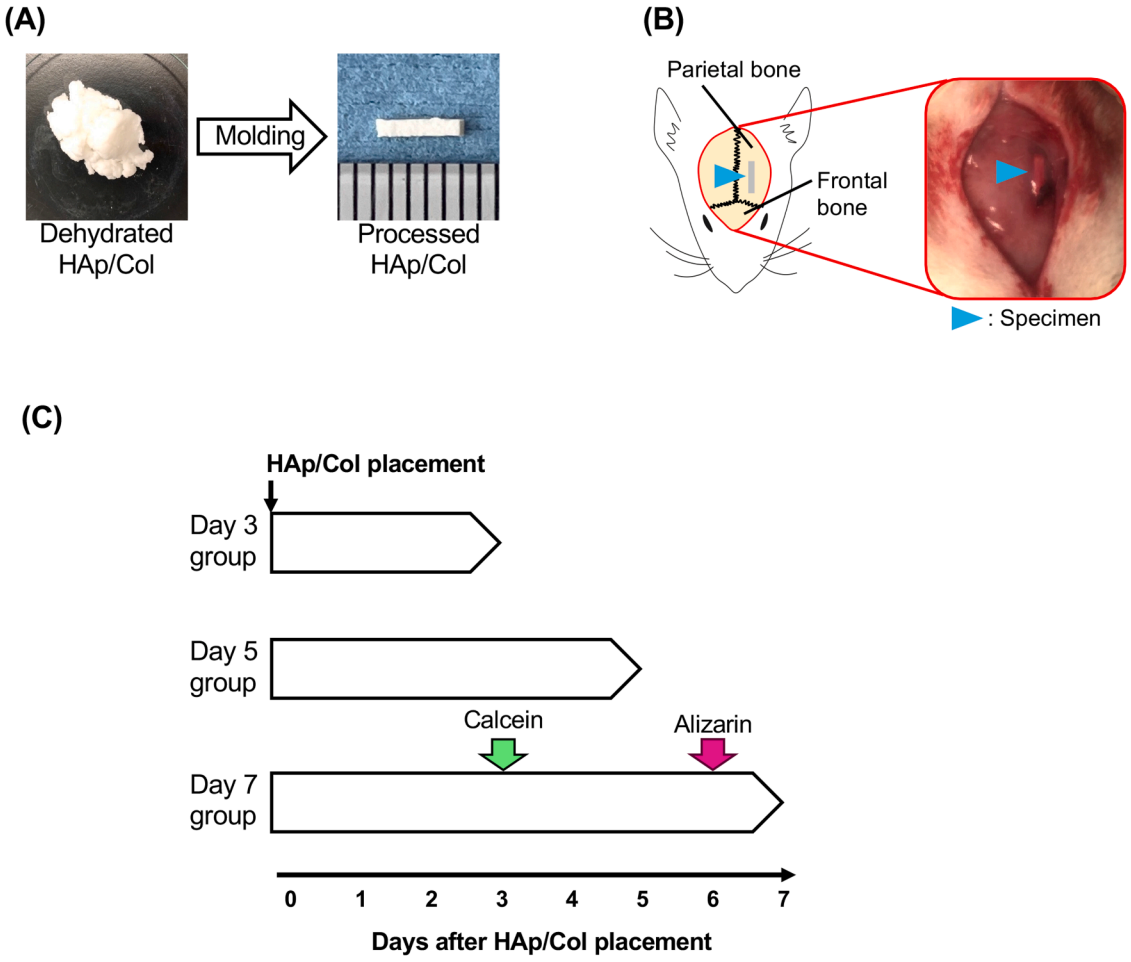

Fig. 1. Experimental design for placing HAp/Col beneath the calvarial periosteum. Preparation of the HAp/Col block. HAp/Col fibers were compressed in a mold, dehydrated, lyophilized, and cut into 1 × 1 × 5 mm rectangles (A). **Schematic diagram of the surgical site on the rat calvaria.** The specimen was inserted under the rat periosteum on the left parietal bone (B). **Experimental timeline.** After specimen placement, samples were collected for histological staining (Von Kossa staining, toluidine blue staining, ALP and TRAP), qRT-PCR, and IHC (CTHRC1 and VEGFR2). For bone morphometry, calcein (0.2 ml/100 g) was administered on day 3 and alizarin complexon (0.2 ml/100 g) on day 6, followed by analysis on day 7 (C).

2.3. Histological observations

Calvarial bone and surrounding soft tissues were sectioned as fresh-frozen samples and fixed with 4% paraformaldehyde at 4°C for 24 h (n = 9). Undecalcified frozen sections (4 μm thick) were prepared perpendicular to the long axis of the specimens using the Kawamoto method with a cryostat (CM-3000, Leica, Wetzlar, Germany). Sections were stained and imaged with an optical microscope (BZ-X810; Keyence, Osaka, Japan).

2.3.1. Von Kossa staining

Sections were immersed in 5% silver nitrate solution (Sigma-Aldrich, St. Louis, MO, USA) for 5 min at room temperature, rinsed with deionized (DI) water, and treated with developer solution for 5 min. After additional rinsing to remove unreacted silver, the sections were immersed in a fixative solution for 5 min.

Sections were then counterstained with Ponceau-Acid Fuchsin (Sigma-Aldrich) solution for 1 min. After counterstaining, the sections were sequentially treated with 1% acetic acid (5 s; FUJIFILM Wako Pure Chemical Corporation, Osaka, Japan), Orange G (1 min; Sigma-Aldrich), and again with 1% acetic acid (5 s). Sections were rinsed DI water between each step. All procedures were performed under light-protected conditions.

2.3.2. Toluidine blue staining

Sections were incubated in 0.1% toluidine blue solution (FUJIFILM Wako) prepared in 0.1 M phosphate buffer (pH 6.8) for 2–5 min at room temperature and rinsed with DI water.

2.3.3. Tartrate-resistant acid phosphatase (TRAP)/ alkaline phosphatase (ALP) double staining

TRAP buffer was prepared by dissolving 11.5 g of sodium tartrate dihydrate (FUJIFILM Wako) and 8.2 g anhydrous sodium acetate (Sigma-Aldrich) in distilled water (DW). The pH was adjusted to 5.0 using 1 N hydrochloric acid (FUJIFILM Wako) or 100% acetic acid, and the volume was brought to 1 L with DW. Naphthol AS-MX phosphate disodium salt (5 mg; FUJIFILM Wako), dissolved in 500 μL of N,N-dimethylformamide (FUJIFILM Wako), was added to 50 mL of the TRAP buffer, followed by 30 mg Fast Red Violet LB salt (Sigma-Aldrich).

Sections were first stained using an ALP staining kit (FUJIFILM Wako) according to the manufacturer's instructions, then immersed in TRAP staining solution and incubated at room temperature for 15–30 min. After staining, sections were counterstained with methyl green (FUJIFILM Wako).

2.4. Gene expression analyses

The HAp/Col region was dissected free from surrounding tissues and homogenized (n = 9). Total RNA was extracted using the total RNA extraction kit (Reliaprep RNA Tissue Miniprep System; Promega Corporation, Madison, WI, USA). Reverse transcription was performed with a reverse transcription master mix (SuperScript™ IV VILO™ Master Mix; Invitrogen, Carlsbad, CA, USA). Quantitative PCR (qPCR) was performed using a Real-Time PCR System (ABI 7300 Real-Time PCR System; Applied Biosystems, Foster City, CA, USA) with SYBR Green Mix (SYBR Green PCR Master Mix; Applied Biosystems). Gene expression of *Cthrc1, Rankl*, and *Runx2* was analyzed by the ΔΔCT method and normalized to *Gapdh*.

Primers were designed using Primer-BLAST, (NCBI of Health, Bethesda, MD, USA) with the following parameters: 18–24 bp length, 58–62 °C melting temperature (Tm), 40–60% GC content, and performance of exon–exon junctions. Primer specificity was confirmed *in silico*. Primer sequences were as follows:

Gapdh: forward 5′- ACTTTGTCAAGCTCATTTCC -3′; reverse 5′- TGCAGCGAACTTTATTGATG -3'

Rankl: forward 5′- AGCCTTTCAAGGGGCCGTGC -3′; reverse 5′- GGGCCACATCGAGCCACGAA -3'

Cthrc1: forward 5′- TTCACAAAGATGCGTTCCAA -3′; reverse 5′- GAAGAGGTCCCGAACATTCA -3'

All primers were synthesized by Thermo Fisher Scientific (Waltham, MA, USA) and verified for specificity and efficiency prior to use.

2.5. Immunohistochemistry (IHC)

The sections prepared by the Kawamoto method were immersed in 100% ethanol and rinsed with DW. Antigen retrieval was performed with HistoVTone (Nacalai Tesque, San Diego, CA, USA) at 70°C for 20 min or ProK at 36°C for 30 min. Endogenous peroxidase activity was blocked with 3% H_2O_2 (Wako, Osaka, Japan) for 30 min at room temperature. After rinsing with PBS containing 0.1% Tween-20 (PBST), Sections were incubated with Anti- vascular endothelial growth factor receptor 2 (VEGFR2) antibody (1:99; ab2349, Abcam, Cambridge, UK). Negative controls were incubated with anti-goat IgG (1:99; AB-108-C, R&D Systems, Minneapolis, MN, USA) at the same concentration as the primary antibody subsequently, staining was performed with HRP-conjugated goat anti-rabbit IgG H&L secondary antibody (1:99; ab6721; Abcam, Cambridge, UK) for 2 h at room temperature. After PBST washing, sections were visualized with DAB (Funakoshi, Tokyo, Japan) for 5 min, and counterstained with methyl green (FUJIFILM Wako) for 1 min. The number of VEGFR2 (+)/TRAP (+) cells was counted by counting the cells that invaded the inside of the swollen HAp/Col.

2.6. Bone histomorphometry

Fluorochrome labeling was performed by intraperitoneal injection of calcein (0.2 mL/100 g; Sigma-Aldrich) on day 3 and alizarin complexone (0.2 mL/100 g; Sigma-Aldrich) on day 6 after implantation. Animals were euthanized on day 7, and specimens with surrounding tissues were collected, fixed, and processed as described in *section 2.3*. Frozen sections were stained as described in *sections 2.3.1–2.3.4*. Labeled sections were imaged by optical microscopy, and bone morphometric parameters were quantified using ImageJ software (version 1.5.3; mac OS, NIH, MD, USA). The mineral apposition rate (MAR) was calculated by measuring the mean distance between the calcein and alizarin labels, divided by the labeling interval (3 days). The MAR within the specimens was determined at the sites of newly formed bone, as shown in Fig. 3-I-A, and was compared with that of the cortical bone controls.

2.7. Statistical analysis

All data were analyzed using "R" software (Version 4.3.1 for macOS, http://www.r-project.org/). One-way ANOVA followed by Tukey's post hoc test, or paired t-tests were applied as appropriate. Statistical significance was defined at $p < 0.05$.

3. Results

3.1. Vascular infiltration into HAp/Col

All rats survived the experimental period without infection. By day 3 post-surgery, VEGFR2-positive cells were observed in the outermost layer and in parts of the HAp/Col scaffold, indicating the onset of vascular invasion (Fig. 2-D, G, d, and g). By day 5, the number of VEGFR2-positive cells increased compared with day 3, extending toward the center of HAp/Col (Fig. 2-E, H, e, and h). By day 7, numerous VEGFR2-positive cells overlapped with the TRAP-positive area at the scaffold periphery, and bone marrow cavity-like structures had formed within HAp/Col (Fig. 2-F, I, f, and i). Quantitative analysis confirmed that the number of VEGFR2(+)/TRAP(+) cells increased progressively from day 3 to day 7, supporting the histological observations (Fig. 2-J). Thus, blood vessel infiltration began by day 3, reached the scaffold

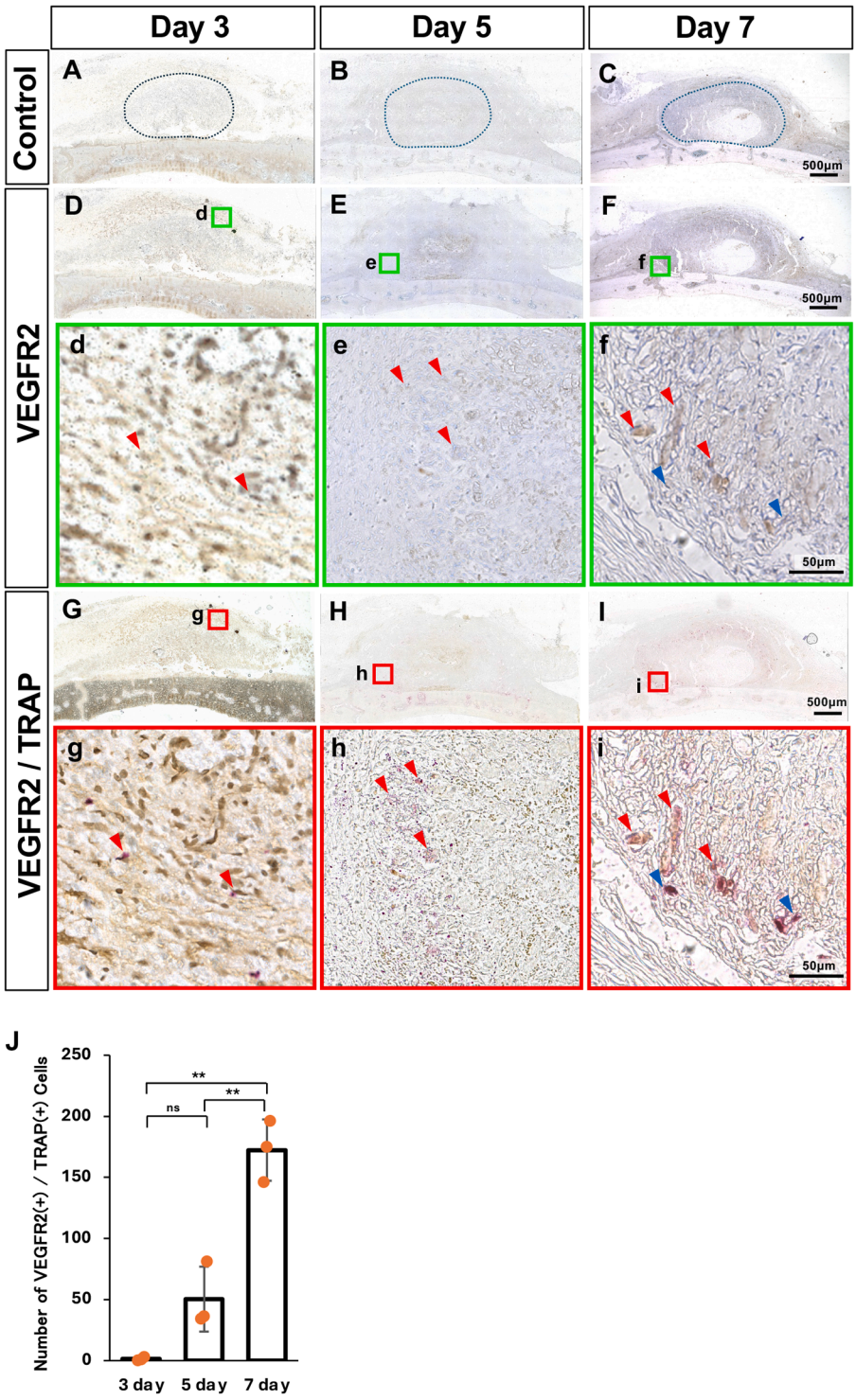

Fig. 2. Vascular invasion into HAp/Col detected by VEGFR2 immunohistochemistry. Frozen sections collected on postoperative days 3, 5, and 7 were stained with anti-VEGFR2 antibody and visualized using DAB chromogen (brown). Positive VEGFR2 staining indicates vascular invasion. Negative controls were incubated with goat IgG at the same concentration as the primary antibody. The gray dashed line indicates the outline of HAp/Col (A-C). VEGFR2 immunostaining confirmed vascular infiltration within the HAp /Col (D-F). Representative high-magnification images of immunostaining for VEGFR2 in the bone formation region (d-f). The same sections were subsequently double-stained with TRAP (G-I). In high-magnification images; red arrowheads indicate TRAP-positive VEGFR2-positive cells, and blue arrowheads indicate TRAP-positive/VEGFR2-negative cells (g-i). The numbers of VEGFR2(+)/TRAP(+) cells were quantified in the region of interest within the HAp/Col (J). Dots represent individual data points. Error bars indicate standard deviation (SD). Statistics: One-way ANOVA with Tukey's post hoc test; paired t-test where indicated. (n=3/group) *p < .05; **p < .01.

center by day 5, and was associated with bone marrow-like cavity formation by day 7 (Fig. 2-D-F, d-f). The external shape of HAp/Col also expanded progressively as blood vessels and various cells infiltrated the scaffold.

3.2. Time-dependent bone formation induced by HAp/Col

Von Kossa staining revealed that, at day 3, HAp nanocrystals in the scaffold were uniformly stained black-brown, with stronger intensity at the outermost layer, suggesting initiation of peripheral calcification (Fig. 3-A). ALP-positive cells were detected outside the expanding scaffold (Fig. 3-G, g1), and a few of ALP-positive osteoblasts infiltrated the interior (Fig. 3-G, g2). By day 5, von Kossa staining at the outer periphery reached its strongest intensity, and staining within the scaffold was more pronounced than on day 3 (Fig. 3-B). ALP activity also increased both inside and outside HAp/Col (Fig. 3-H). Osteoblasts on the outside of HAp/Col showed elongated morphology aligned with the expansion direction (Fig. 3-h1), while those inside were arranged along the endosteal side of vascular spaces (Fig. 3-h2).

On day 7, von Kossa staining further intensified compared with day

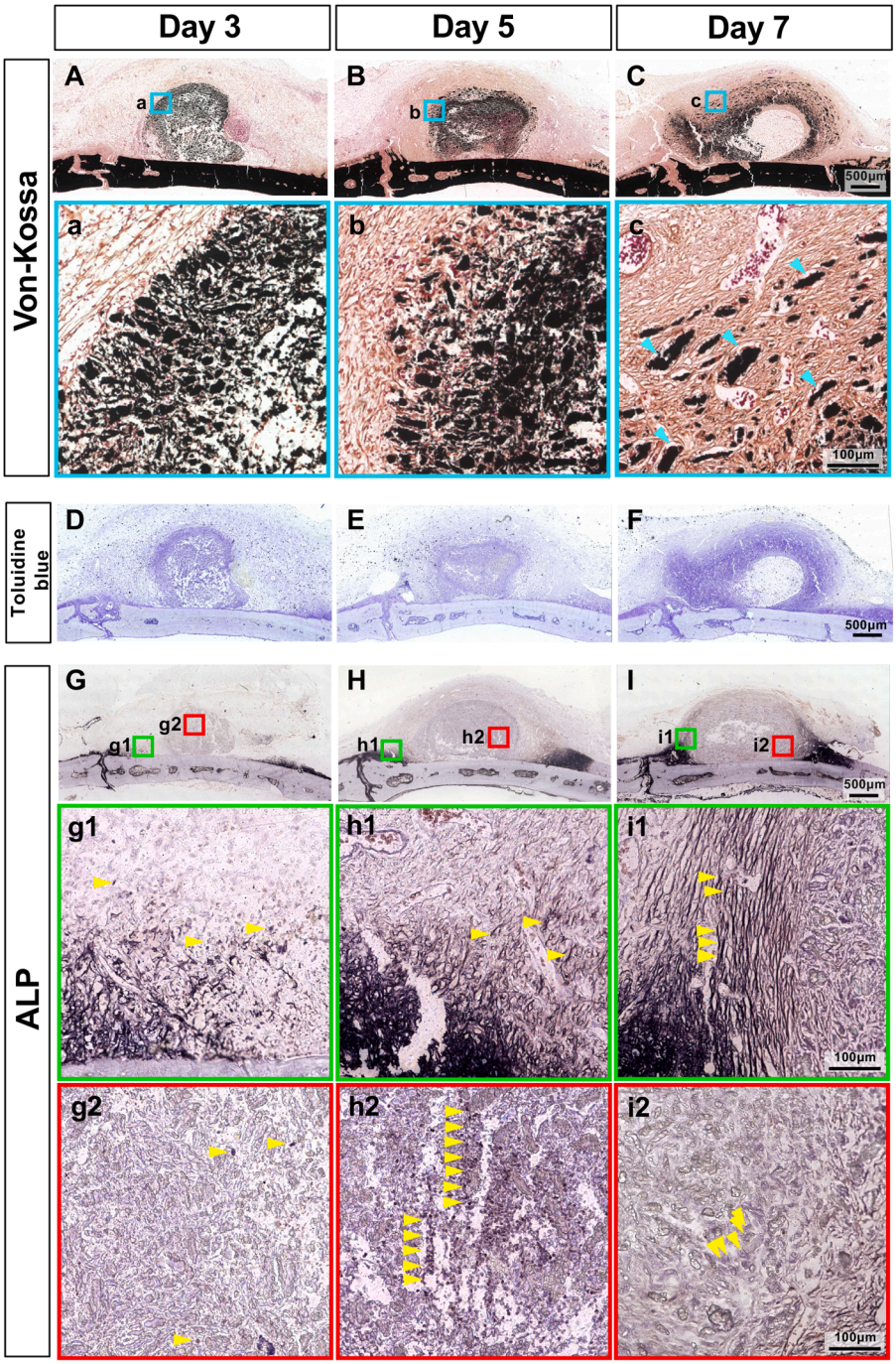

Fig. 3. Histological staining of time-dependent new bone formation induced by HAp/Col. Von Kossa (A-C, and a-c), Toluidine blue (D-F), and ALP (G-I, g1-i1, and g2-i2) staining on days 3, 5, and 7 after HAp/Col placement. Representative high-magnification images of Von Kossa staining (a-c). On day 3, HAp nanocrystals stained uniformly; round osteoblasts appeared around the specimen (g1), with early infiltration along vessels (g2). By day 5, elongated osteoblasts surrounded the specimen (h1) and lined vascular cavity inside (h2). On day 7, elongated osteoblasts morphology formed along the outer surface due to HAp/Col swelling, (i1), while large osteoblasts appeared internally (i2).

5, and concentric islands of calcified tissue were observed near the periphery (Fig. 3-C). Osteoblasts extended toward the scaffold center and actively synthesized bone matrix (Fig. 3-i1). Outside the scaffold, bone formation appeared as a thickened ALP-positive osteoblast layer on the skull surface, with cells extending upward (Fig. 3-i2). Toluidine blue staining confirmed the absence of cartilage-like tissue, indicating membranous ossification, a process that enables rapid bone formation (Fig. 3-D-F).

The number of osteoblasts per bone volume (N. Ob/BV) increased from 3 to 5 days, and bone formation continued to increase up to day 7 (Fig. 4-II-A). Bone histomorphometry with alizarin/calcein double labeling coupled with ALP staining revealed progressive bone formation from the scaffold surface toward the interior along vascular invasion (Fig. 4-I-a-b). With respect to the mineral apposition rate (MAR), no statistically significant difference was detected between the values observed within the HAp/Col and those in the cortical bone distant from the HAp/Col (Fig. 4-II-B). Around the HAp/Col, measurement of the fluorescent area within 500 μm from the advancing front of the newly formed surrounding bone showed that the alizarin-labeled area was significantly larger than the calcein-labeled area (Fig. 4-II-C). Bone extended outward from HAp/Col in its expanding direction, whereas infiltrating inward within the scaffold (Fig. 4-I-a-b). The osteogenic marker *Rankl* increased gradually from days 3 to 7, although differences were not statistically significant (Fig. 4-II-D).

3.3. Osteoclastic resorption of biomaterials over time

The progressive increase in the number of osteoclasts per mm of bone surface (N. Oc/BV) up to day 7 indicated enhanced bone resorption (Fig. 5-I-A). On day 3, VEGFR2(+)/TRAP(+) cells appeared on the scaffold surface, suggesting early HAp/Col resorption (Fig. 2-g). A small number of osteoclasts also infiltrated into the scaffold (Fig. 5-I-B, C). By day 5, TRAP(+) multinucleated osteoclasts were observed in the outer periphery of HAp/Col, coinciding with regions of vascular invasion (Fig. 2-h; Fig. 5-I-a1-c1). By day 7, both VEGFR2(+)/TRAP(+) endothelial-like osteoclasts and VEGFR2(-)/TRAP(+) macrophage-derived osteoclasts were detected, actively osteoclastic resorbing HAp/Col and contributing bone remodeling (Fig. 2-i; Fig. 5-I-a2-c2).

RT-qPCR analysis revealed *Cthrc1* mRNA expression, reported as a coupling factor, increased over time in cells within HAp/Col (Fig. 5-II-B).

4. Discussion

4.1. Bone formation in and around HAp/Col

HAp/Col was implanted beneath the rat periosteum using a rat skull model to assess its biological behavior. Temporal changes in bone formation and resorption activity were evaluated by bone morphometry.

By day 3, VEGFR2-positive and TRAP-positive cells were detected, indicating early sinusoidal capillary infiltration into the skull. At the same time, von Kossa staining was more pronounced at the outer periphery of HAp/Col, and elongated ALP-positive cells with calcein-labeling suggested that onset of immature new bone formation in the same region. *Rankl* expression increased over time, reflecting enhanced osteoclast differentiation. PCR results remained unstable until day 5, likely due to rapid local biological changes. Since RANKL levels are typically low in mesenchymal stem and osteoblastic precursor cells [8], the qRT-PCR data suggested that osteoblasts had reached a more differentiated and mature state by day 7.

4.2. Promotion of bone formation by vascular invasion

Vascular invasion into HAp/Col was observed by day 3, and bone marrow cavity-like structure appeared in its center by day 7 (Fig. 2-F). Consistent with earlier findings [9], endochondral ossification-like

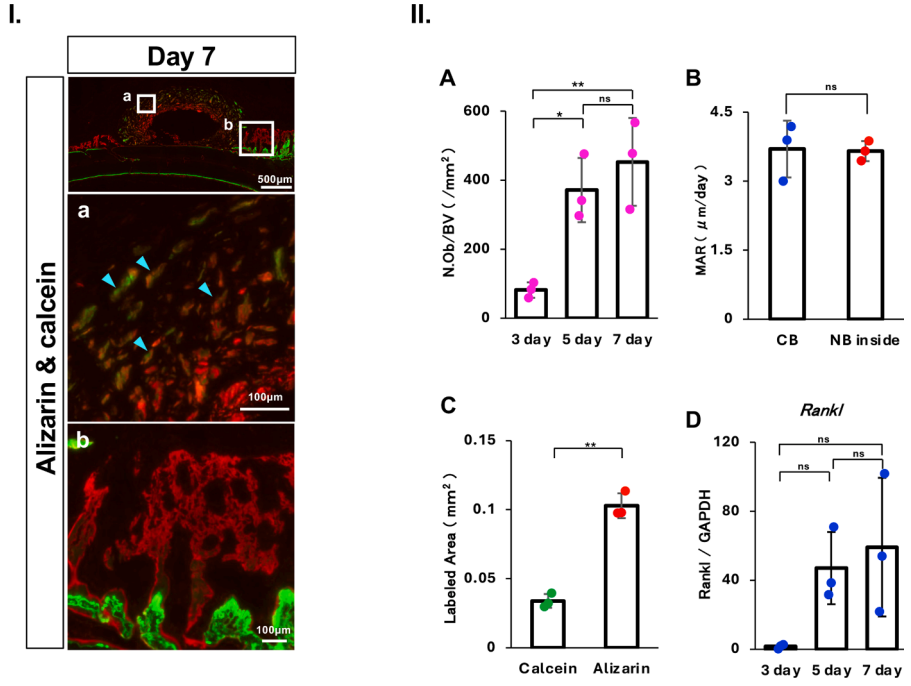

Fig. 4. Fluorescent double labeling and quantitative analysis of time-dependent new bone formation induced by HAp/Col. I. Fluorescent double labeling. Calcein (0.2 ml/100 g) was injected on day 3 and alizarin complexon (0.2 ml/100 g) on day 6. Double labelling shows bone formation progressing inside the scaffold (a) and new bone formation from the periphery inward (b). **II. Quantitative analysis.** Osteoblast number per bone volume (N.Ob/BV) inside the HAp/Col (A). Mineral apposition rate (MAR) within specimens compared to cortical bone controls (B). Labeled area outside the scaffold (C). RT-qPCR analysis of *Rankl* expression in cells invading the swollen scaffold (D). Dots represent individual data points. Error bars indicate standard deviation (SD). Statistics: One-way ANOVA with Tukey's post hoc test; paired t-test where indicated. (n=3/group) *p < .05; **p < .01 Light blue arrowheads indicate newly formed bone in an island-like pattern; and yellow arrowheads indicate osteoblasts.

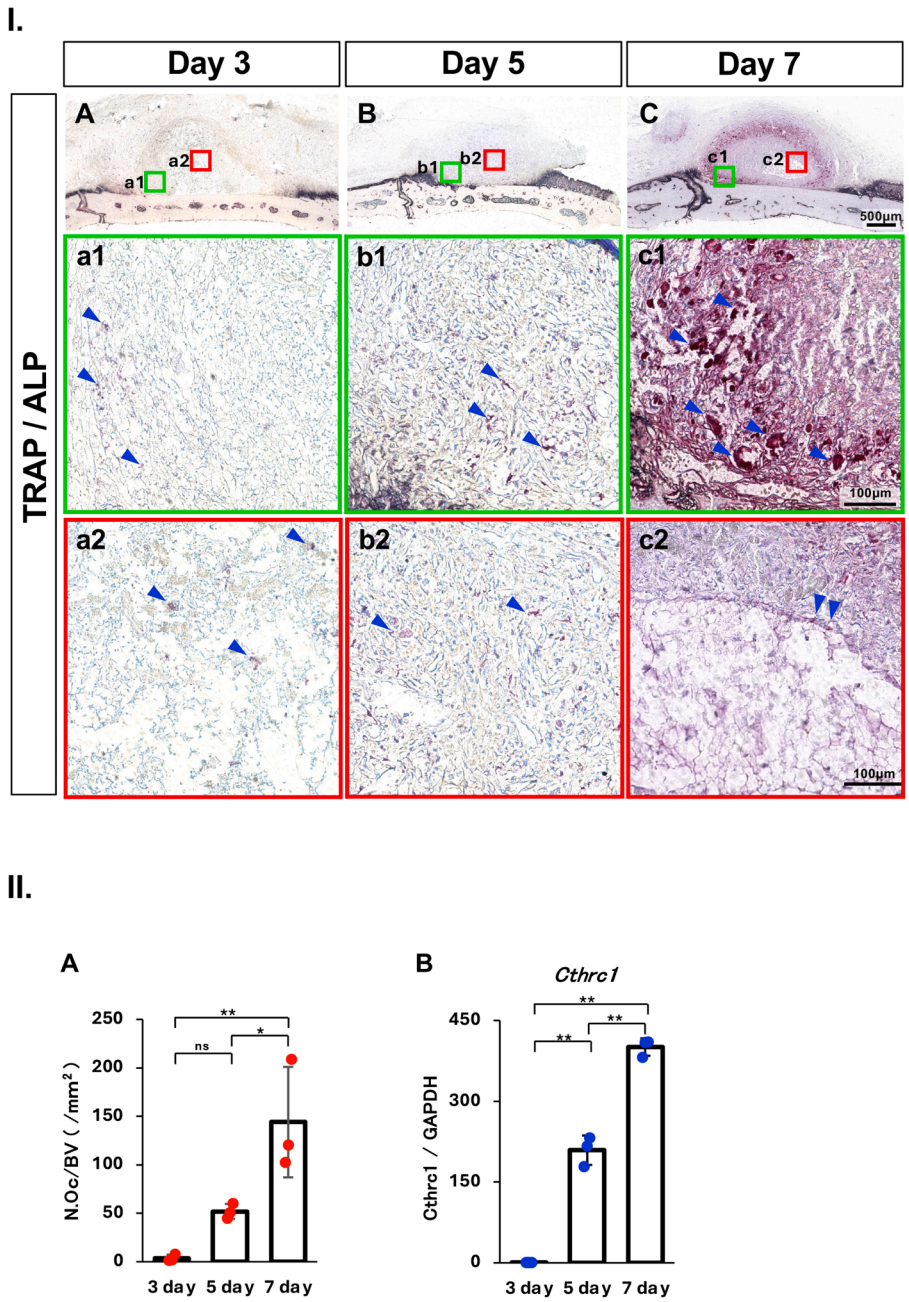

Fig. 5. Bone remodeling activity after HAp/Col placement. I. TRAP/ALP double staining. On day 3, osteoclasts were observed near blood vessels externally and within the scaffold (A, and a1-a2). By day 5, osteoblast accumulation increased towards the center (B, and b1-b2). On day 7 (C, and c1-c2), mature osteoclasts actively resorbing bone appeared at the periphery (c1) and on the inner surfaces of marrow-like cavities (c2). Arrowheads indicates osteoclasts within the specimens. **II. Quantitative analysis.** Osteoclast number per bone volume (N.Oc/BV) within the scaffold (A). RT-qPCR analysis of *Cthrc1* expression in invading cells (B). Dots represent individual data points. Error bars indicate standard deviation (SD). Statistics: one-way ANOVA with Tukey's post hoc test. (n=3/group) *p < .05; **p < .01.

tissue, including marrow cavity tissue, formed within the HAp/Col. This closely resembled natural endochondral ossification, where cartilage is resorbed by chondrocytes and replaced with primary cancellous bone [10].

Angiogenesis and osteogenesis are generally linked through VEGF production under hypoxic conditions, mediated by hypoxia-inducible factor (HIF) transcription factors [11]. However, Bixel et al. reported that natural healing of small calvarial defects, vascular regeneration preceded bone regeneration, suggesting the two processes may not be coupled in the early repair [12]. Nonetheless, VEGF is essential for skeletal development and bone repair *in vivo*. Its receptors, VEGFR1 and VEGFR2, play critical roles in angiogenesis during endochondral ossification, and inhibition of VEGF by administering a soluble chimeric VEGF receptor protein suppressed vascular invasion into the hypertrophic zone of the long bone growth plate and cancellous bone formation [13].

In vitro, VEGF and RANKL promoted osteoclastogenesis in hematopoietic stem cells [14]. Particularly, osteoblast-derived VEGF stimulates blood vessel recruitment and cartilage resorption in the early stage, while promoting osteoclast-mediated bone remodeling in the later stage of endochondral ossification during bone repair [15].

By day 3, TRAP(+)/VEGFR2(+) osteoclasts associated with sinusoidal capillaries, together with ALP-positive cells, had infiltrated the periphery of the specimens (Fig. 2-G, g; Fig. 3-g2). By day 7, some TRAP(+)/VEGFR2(+) osteoclasts remained at the periphery of HAp/Col, while TRAP(+)/VEGFR2(-) mature osteoclasts were also observed

around bone marrow cavity-like structure in the center (Fig. 2-I, i). These observations suggest that the recruitment of vascular endothelial cells and mesenchymal stem cells within the scaffold may contribute to ongoing bone formation and remodeling in HAp/Col.

In a previous subperiosteal calvarial study using the same experimental model, Hiratsuka et al. reported that β-TCP primarily supported bone formation along the material surface, while cellular infiltration into the scaffold interior was limited [7]. In contrast, HAp/Col was shown to permit internal distribution of TRAP-positive cells and osteoblasts, although angiogenic processes were not directly evaluated in that study. The present findings extend these observations by providing direct histological evidence of early VEGFR2-positive vascular--associated cell infiltration preceding osteoblast localization within the scaffold interior, suggesting a mechanistic basis for the internal remodeling-like events reported previously.

4.3. Bone formation outside HAp/Col

Outside HAp/Col, osteoblasts adjacent to basal bone adhered directly to the material and initiated bone formation, consistent with reports that osteoblasts preferentially adhere to collagen fibers aligned parallel to bone surface [9].

A critical requirement of biomaterials is their space-forming ability [16]. We hypothesized that HAp/Col, placed beneath the periosteum, was subjected to external mechanical stimulation, promoting osteogenesis via traction forces. As cellular infiltration and vascularization progressed, the material expanded, intensifying these forces. Notably, ALP-positive cells aligned with the traction direction, supporting the role of sustained mechanical stimulation in per-material bone formation (Fig. 3-g1-i1). Conversely, compressed top and bottom surfaces showed no additional bone or MAR increase (Fig. 3-G-I). These findings suggest that osteoblast-mediated bone formation is promoted under tension but suppressed under compression. Supporting this, Hiratsuka *et al.* found greater bone formation in swollen HAp/Col than in β-TCP, suggesting superior osteoconductivity due to its collagen content [7].

4.4. Promotion of bone formation by osteoblasts that invade inside HAp/Col

Kimura *et al.* showed that forkhead box G1 (Foxg1), a regulator for ALP activity and master genes for osteoblast differentiation, including osteocalcin, Col1α1, and osterix, enhances *Runx2* mRNA expression in the presence of the collagen-derived dipeptide prolylhydroxyproline (Pro-Hyp) [17]. Furthermore, Pro-Hyp directly binding to Foxg1, further increasing Runx2 expression [18]. Based on these previous findings, it is plausible that collagen degradation within HAp/Col may release Pro-Hyp, which activates Foxg1 in osteoblasts adhering to the scaffold, thereby promoting bone formation via Runx2 signaling.

In this study, scattered ALP-positive osteoblasts were detected within HAp/Col on day 3 (Fig. 3-g2). By day 5, these osteoblasts formed continuous along voids resembling vascular cavities (Fig. 3-h2). By day 7, the clusters displayed enlarged cytoplasm and active bone matrix production (Fig. 3-i2), indicating progressive osteoblast differentiation and function within scaffold.

4.5. Promotion of bone formation by HAp/Col involved through CTHRC1

HAp/Col blocks gradually expand under physiological pH, with their surfaces gradually acquiring a gel-like texture. When implanted into rat calvaria, the bone mineral content (BMC) of HAp/Col decreased progressively, accompanied by an increase in local calcium ion concentration [7]. HAp/Col has also been reported to induce osteoclastogenesis [19], likely because collagen fragments bind to OSCAR, which associates with Fc receptors (FcRs) on osteoclast precursors, elevating intracellular calcium and promoting osteoclast differentiation and maturation [20]. Based on these mechanisms, we hypothesized that CTHRC1 contribute to bone formation at sites distant from HAp/Col. CTHRC1 is secreted by osteoclasts in response to elevated calcium and has been shown to promote osteoblast differentiation [21].

CTHRC1 is recognized as a positive regulator of osteogenesis both *in vivo* and *in vitro*. Kimura *et al.* reported that it functions as an autocrine factor stimulating osteoblast proliferation and differentiation in primary bone marrow stromal cells [22]. Similarly, Takeshita *et al.* have reported that mature osteoclasts express CTHRC1, which in turn promotes osteogenesis in calvarial osteoblasts [21]. In contrast, Jin *et al.* reported CTHRC1 expression in osteoblasts and osteocytes, but not in osteoclasts [23]. In this study, CTHRC1-positive regions consistently overlapped with osteoblast-mediated bone formation at days 3, 5, and 7 (Fig. S1). Both the number of osteoblasts and *Cthrc1* mRNA expression increased over time (Fig. 4-II-A; Fig. 5-II-B). Although osteoblast proliferation plateaued between days 5 and 7, *Cthrc1* mRNA expression continued to rise, suggesting enhanced CTHRC1 secretion per cell. The presence of enlarged vesicles and elevated CTHRC1 mRNA expression in osteoblasts further supports this interpretation (Fig. 5-II-B) [24].

The present study did not include functional experiments to directly verify the roles of CTHRC1. However, this study was conducted in rats, and knockout experiments would require the use of mice. Since the specimens in this study were extremely small and precisely sectioned, adjusting their size and handling for mouse experiments would be technically difficult. Therefore, their mechanistic contribution to bone regeneration should be interpreted with caution and confirmed in future studies.

4.6. Clinical implications

Adequate alveolar bone height and width are critical for safe tooth movement and dental implant placement, as the alveolar bone serves as the primary supporting tissue. However, many clinical situations, such as thin alveolar bone, age related bone loss, and congenital defects such as cleft palate, are characterized by insufficient alveolar bone volume. These limitations often restrict treatment planning.

Bone regenerative techniques using biomaterials such as HAp/Col offer a promising strategy for augmenting alveolar bone volume. Such approaches could expand treatment options for adult patients and individuals with cleft alveoli by enabling the reconstruction of continuous alveolar bone.

This study provides preliminary preclinical information on the early tissue responses to the subperiosteal placement of HAp/Col. The observed vascular infiltration and coordinated cellular activities suggest that HAp/Col may provide a biologically permissive environment for periosteal bone formation. However, because this study was short-term and did not include a contemporaneous control group, these findings should be interpreted as descriptive in nature.

4.7. Limitations

This study has several limitations. First, although VEGFR2-positive cells infiltrated the HAp/Col scaffold from day 3, inhibition experiments were not performed. Therefore, the direct contribution of VEGFR2 to angiogenesis within the HAp/Col scaffold remains undetermined and should be clarified in future studies.

Second, this study did not include functional experiments to directly verify the roles of CTHRC1. Although bone-specific Cthrc1 conditional knockout models have been reported, conducting genetic studies using these models was beyond the scope of the present work [21]. Future investigations employing appropriate conditional knockout approaches will be necessary to clarify the mechanistic contribution of CTHRC1 to bone regeneration.

Third, this study did not include a separate control material. Previous studies used β-TCP as a control and demonstrated that β-TCP exhibits minimal cellular infiltration within the scaffold interior during the first seven days after subperiosteal placement. In contrast, the present study

was designed to evaluate, in a time-resolved and descriptive manner, the early sequence of vascular infiltration and the coupled osteoclast–osteoblast responses occurring within HAp/Col under a standardized subperiosteal environment. For this reason, we did not perform direct material-to-material comparisons. Instead, we interpreted our findings within the context of previously published subperiosteal studies, including those involving β-TCP. Nevertheless, the absence of a contemporaneous control group limits the direct interpretation of material-specific effects.

Finally, several statistical considerations related to sample size and power should be acknowledged [25]. In this study, effect sizes for the ANOVA were quantified using η^2, defined as the ratio of between-group sum of squares to the total sum of squares:

$$\eta^2 = \frac{SS_{\text{between}}}{SS_{\text{total}}}$$

Cohen's f was calculated from η^2 as follows:

$$f = \sqrt{\frac{\eta^2}{1-\eta^2}}$$

Post hoc power analyses were performed using these effect sizes. For the main outcome (N.Ob/BV), the large effect size ($\eta^2 = 0.82$) resulted in sufficiently high statistical power. In contrast, Rankl mRNA exhibited a moderate-to-large effect size ($\eta^2 = 0.57$), and some pairwise comparisons—particularly between day 5 and day 7—showed low statistical power due to small standardized mean differences. The required sample size to achieve 80% power for each pairwise comparison was estimated using the standard formula for two-sample comparisons:

$$n = \frac{2\left(Z_{1-\alpha/2} + Z_{1-\beta}\right)^2}{d^2}$$

where d is Cohen's d, $Z_{1-\alpha/2}$ is the critical value for the significance threshold, and $Z_{1-\beta}$ corresponds to the desired power. For the comparison between day 5 and day 7, the very small effect size ($d = 0.38$) resulted in an estimated requirement of $n = 110$ per group, which was not feasible due to practical, ethical, and resource-related constraints associated with in vivo experimentation. These statistical limitations should be considered when interpreting the Rankl mRNA results.

5. Conclusion

This study demonstrated time-dependent vascular invasion and the presence of osteoclast- and osteoblast-associated activities within HAp/Col in a rat calvarial model. These biological responses were consistent with physiological bone remodeling processes and did not indicate adverse tissue reactions. Collectively, HAp/Col demonstrates biocompatibility and safety as a candidate material for medical and orthodontic applications.

Funding

This work was supported by MEXT, the establishment of university fellowship toward the creation of science technology innovation, and the Japan Society for the Promotion of Science (JSPS) KAKENHI Grant No. 21K17177.

CRediT authorship contribution statement

Hanae Arai: Writing – original draft, Visualization, Methodology, Investigation, Formal analysis, Data curation. **Masayoshi Uezono:** Writing – review & editing, Validation, Supervision, Software, Resources, Project administration, Methodology, Funding acquisition, Formal analysis, Conceptualization. **Masanori Kikuchi:** Writing – review & editing, Resources, Methodology. **Hitoshi Amano:** Writing – review & editing, Methodology, Investigation, Formal analysis. **Chen Derong:** Investigation, Formal analysis, Data curation. **Kazuhiro Aoki:** Writing – review & editing, Visualization, Supervision, Resources. **Keiji Moriyama:** Writing – review & editing, Resources, Project administration.

Declaration of competing interest

The authors declare no conflicts of interest.

Acknowledgments

This work was supported by the Department of Maxillofacial Orthognathics and Department of Basic Oral Health Engineering. Micro-CT analyses were performed at the Research Core of Institute of Science Tokyo. I would like to thank Professor Toshiyuki Ikoma for helpful discussions and suggestions, and Li Bin for technical advice with immunohistochemistry. The authors gratefully acknowledge Dr. Takeshi Ogasawara and Dr. Satoka Takeuchi, Department of Maxillofacial Orthognathics, Institute of Science Tokyo, for their valuable advice and insightful discussions.

Supplementary materials

Supplementary material associated with this article can be found, in the online version, at doi:10.1016/j.bbiosy.2026.100130.

Data availability

The datasets generated and analyzed during the current study are available from the corresponding author upon reasonable request. The data have not been deposited in a public repository because deposition was not required at the time of the study, but the authors are willing to share them upon request.

References

[1] Kikuchi M, Itoh S, Ichinose S, Shinomiya K, Tanaka J. Self-organization mechanism in a bone-like hydroxyapatite/collagen nanocomposite synthesized in vitro and its biological reaction in vivo. Biomaterials 2001;22(13):1705–11. https://doi.org/10.1016/s0142-9612(00)00305-7.

[2] Kawamoto T. Use of a new adhesive film for the preparation of multi-purpose fresh-frozen sections from hard tissues, whole-animals, insects and plants. Arch Histol Cytol 2003;66(2):123–43. https://doi.org/10.1679/aohc.66.123.

[3] Sotome S, Ae K, Okawa A, Ishizuki M, Morioka H, Matsumoto S, Nakamura T, Abe S, Beppu Y, Shinomiya K. Efficacy and safety of porous hydroxyapatite/type 1 collagen composite implantation for bone regeneration: a randomized controlled study. J Orthop Sci 2016;21(3):373–80. https://doi.org/10.1016/j.jos.2016.01.007.

[4] Dam VV, Trinh HA, Rokaya D, Trinh DH. Bone Augmentation for implant placement: recent advances. Int J Dent 2022;2022:8900940. https://doi.org/10.1155/2022/8900940.

[5] Block MS, Hoffman DR. A new device for absolute anchorage for orthodontics. Am J Orthod Dentofacial Orthop 1995;107(3):251–8. https://doi.org/10.1016/s0889-5406(95)70140-0.

[6] Uezono M, Takakuda K, Kikuchi M, Suzuki S, Moriyama K. Hydroxyapatite/collagen nanocomposite-coated titanium rod for achieving rapid osseointegration onto bone surface. J Biomed Mater Res B Appl Biomater 2013;101(6):1031–8. https://doi.org/10.1002/jbm.b.32913.

[7] Hiratsuka T, Uezono M, Takakuda K, Kikuchi M, Oshima S, Sato T, Suzuki S, Moriyama K. Enhanced bone formation onto the bone surface using a hydroxyapatite/collagen bone-like nanocomposite. J Biomed Mater Res B Appl Biomater 2020;108(2):391–8. https://doi.org/10.1002/jbm.b.34397.

[8] Furuya Y, Inagaki A, Khan M, Mori K, Penninger JM, Nakamura M, Udagawa N, Aoki K, Ohya K, Uchida K, Yasuda H. Stimulation of bone formation in cortical bone of mice treated with a receptor activator of nuclear factor-κB ligand (RANKL)-binding peptide that possesses osteoclastogenesis inhibitory activity. J Biol Chem 2013;288(8):5562–71. https://doi.org/10.1074/jbc.M112.426080.

[9] Sakakibara M, Hasegawa T, Haraguchi-Kitakamae M, Shi Y, Li W, Cui J, Liu X, Yamamoto T, Hongo H, Amizuka N, Sato Y, Kikuchi M. Histochemical analysis of osteoclast and osteoblast distributions on hydroxyapatite/collagen bone-like nanocomposite embedded in rat tibiae. J Oral Biosci 2025;67(1):100612. https://doi.org/10.1016/j.job.2025.100612.

[10] Maes C, Kobayashi T, Selig MK, Torrekens S, Roth SI, Mackem S, Carmeliet G, Kronenberg HM. Osteoblast precursors, but not mature osteoblasts, move into

developing and fractured bones along with invading blood vessels. Dev Cell 2010; 19(2):329–44. https://doi.org/10.1016/j.devcel.2010.07.010.
[11] Schipani E, Maes C, Carmeliet G, Semenza GL. Regulation of osteogenesis-angiogenesis coupling by HIFs and VEGF. J Bone Miner Res 2009;24(8):1347–53. https://doi.org/10.1359/jbmr.090602.
[12] Bixel MG, Sivaraj KK, Timmen M, Mohanakrishnan V, Aravamudhan A, Adams S, Koh BI, Jeong HW, Kruse K, Stange R, Adams RH. Angiogenesis is uncoupled from osteogenesis during calvarial bone regeneration. Nat Commun 2024;15(1):4575. https://doi.org/10.1038/s41467-024-48579-5.
[13] Gerber HP, Vu TH, Ryan AM, Kowalski J, Werb Z, Ferrara N. VEGF couples hypertrophic cartilage remodeling, ossification and angiogenesis during endochondral bone formation. Nat Med 1999;5(6):623–8. https://doi.org/10.1038/9467.
[14] Niida S, Kaku M, Amano H, Yoshida H, Kataoka H, Nishikawa S, Tanne K, Maeda N, Kodama H. Vascular endothelial growth factor can substitute for macrophage colony-stimulating factor in the support of osteoclastic bone resorption. J Exp Med 1999;190(2):293–8. https://doi.org/10.1084/jem.190.2.293.
[15] Hu K, Olsen BR. Osteoblast-derived VEGF regulates osteoblast differentiation and bone formation during bone repair. J Clin Invest 2016;126(2):509–26. https://doi.org/10.1172/JCI82585.
[16] Zakaria O, Madi M, Kasugai S. A novel osteogenesis technique: the expansible guided bone regeneration. J Tissue Eng 2012;3(1):2041731412441194. https://doi.org/10.1177/2041731412441194.
[17] Kimira Y, Odaira H, Nomura K, Taniuchi Y, Inoue N, Nakatani S, Shimizu J, Wada M, Mano H. Collagen-derived dipeptide prolyl-hydroxyproline promotes osteogenic differentiation through Foxg1. Cell Mol Biol Lett 2017;22:27. https://doi.org/10.1186/s11658-017-0060-2.
[18] Nomura K, Kimira Y, Osawa Y, Shimizu J, Kataoka-Matsushita A, Mano H. Collagen-derived dipeptide prolyl hydroxyproline directly binds to Foxg1 to change its conformation and inhibit the interaction with Runx2. Biosci Biotechnol Biochem 2019;83(11):2027–33. https://doi.org/10.1080/09168451.2019.1642099.
[19] Kikuchi M. Hydroxyapatite/collagen bone-like nanocomposite. Biol Pharm Bull 2013;36(11):1666–9. https://doi.org/10.1248/bpb.b13-00460.
[20] Barrow AD, Raynal N, Andersen TL, Slatter DA, Bihan D, Pugh N, Cella M, Kim T, Rho J, Negishi-Koga T, Delaisse JM, Takayanagi H, Lorenzo J, Colonna M, Farndale RW, Choi Y, Trowsdale J. OSCAR is a collagen receptor that costimulates osteoclastogenesis in DAP12-deficient humans and mice. J Clin Invest 2011;121(9):3505–16. https://doi.org/10.1172/JCI45913.
[21] Takeshita S, Fumoto T, Matsuoka K, Park KA, Aburatani H, Kato S, Ito M, Ikeda K. Osteoclast-secreted CTHRC1 in the coupling of bone resorption to formation. J Clin Invest 2013;123(9):3914–24. https://doi.org/10.1172/JCI69493.
[22] Kimura H, Kwan KM, Zhang Z, Deng JM, Darnay BG, Behringer RR, Nakamura T, de Crombrugghe B, Akiyama H. Cthrc1 is a positive regulator of osteoblastic bone formation. PLoS One 2008;3(9):e3174. https://doi.org/10.1371/journal.pone.0003174.
[23] Jin YR, Stohn JP, Wang Q, Nagano K, Baron R, Bouxsein ML, Rosen CJ, Adarichev VA, Lindner V. Inhibition of osteoclast differentiation and collagen antibody-induced arthritis by CTHRC1. Bone 2017;97:153–67. https://doi.org/10.1016/j.bone.2017.01.022.
[24] Machibya FM, Zhuang Y, Guo W, You D, Lin S, Wu D, Chen J. Effects of bone regeneration materials and tooth movement timing on canine experimental orthodontic treatment. Angle Orthod 2018;88(2):171–8. https://doi.org/10.2319/062017-407.
[25] Cohen J. Statistical power analysis for the behavioral sciences. New York: Academic Press; 1977. p. 273–88. Chapter 8.